Synthesis of In_2O_3 Nanowire-Decorated Ga_2O_3 Nanobelt Heterostructures and Their Electrical and Field-Emission Properties

Jing Lin,* Yang Huang,* Yoshio Bando, Chengchun Tang, Chun Li, and Dmitri Golberg

International Center for Materials Nanoarchitectonics (MANA), National Institute for Materials Science, Namiki 1-1, Tsukuba, Ibaraki 305-004, Japan

ABSTRACT We report on the synthesis of In_2O_3 nanowire-decorated Ga_2O_3 nanobelt heterostructures via a simple catalyst-free method. A typical heterostructure, where an In_2O_3 nanowire forms a sort of a "dorsal fin" on the Ga_2O_3 nanobelt, exhibits the T-shaped cross-section. The structure, electrical porperties, and field-emission properties of this material are systematically investigated. The heterostructures possess a typical n-type semiconducting behavior with enhanced conductivity. Field-emission measurements show that they have a low turn-on field (~1.31 V/μm) and a high field-enhancement factor (over 4000). The excellent field-emission characteristics are attributed to their special geometry and good electrical properties. The present In_2O_3-decorated Ga_2O_3 heterostructures are envisaged to be decent field-emitters useful in advanced electronic and optoelectronic nanodevices.

KEYWORDS: Ga_2O_3 nanobelt · In_2O_3 nanowire · heterostructures · electrical properties · field-emission

*Address correspondence to lin.jing@nims.go.jp, huang.yang@nims.go.jp

Received for review February 7, 2010 and accepted March 18, 2010.

10.1021/nn100254f

One-dimensional (1D) semiconductor heterostructured submicrometer/nanometer-scale materials are of prime interest as building blocks in miniaturized electronic and photonic devices.[1] Recently, significant progress has been made in regard to various axial,[2,3] radial,[4−8] and branched[9−12] 1D heterostructure syntheses. In fact, the successful design and controllable growth of composition-modulated heterostructures may lead to enhanced functionalities, such as emission efficiency and high electron mobility.[13] For example, InAs/InP core/shell nanowire heterostructures have shown a significant increase in electron mobility due to the InP passivation layer.[7] ZnS nanotube−In nanowire-branched heterostructures have exhibited multiply enhanced field-emission properties due to their special geometry. Branched structures attached on a long backbone and having effectively high aspect ratios have demonstrated remarkably large field enhancement.[12] All these exciting works indicate that a design of novel 1D heterostructures opens up new wide opportunities not only for fundamental science but also for potential utilizations in diverse functional devices.

Monoclinic gallium oxide (β-Ga_2O_3), one of the transparent conducting oxides, is an important wide band gap material. It becomes an n-type semiconductor when synthesized under reducing conditions due to oxygen vacancies.[14] β-Ga_2O_3 has been considered as a promising material for fabricating optoelectronic devices, spin-tunneling junctions, and gas sensors.[15−18] Although many studies have been devoted to the synthesis and property investigations of various Ga_2O_3 nanostructures, such as wire-, ribbon-, cable-, and cactus-like structures,[14,19−23] the analogous reports on 1D Ga_2O_3-based heterostructures have still been lacking. It is believed that the rational synthesis of such heterostructures will allow one to combine different and distinct functionalities of the components and to realize unique properties in such complex systems.

In this paper, we report on the synthesis of 1D In_2O_3-decorated Ga_2O_3 heterostructures where an In_2O_3 nanowire is located on the back of a Ga_2O_3 nanobelt, thus creating a sort of a "dorsal fin". The heterostructures have widths of ~200−500 nm and lengths of up to tens or hundreds of micrometers. Field-effect transistors (FETs) were designed and fabricated based on individual In_2O_3-decorated Ga_2O_3 heterostructures, and their electrical transport properties were then studied. They exhibited a typical n-type semiconducting behavior and a notable enhancement of conductivity. Moreover, the regarded heterostructures possessed excellent field-emission characteristics: a low turn-on field (~1.31

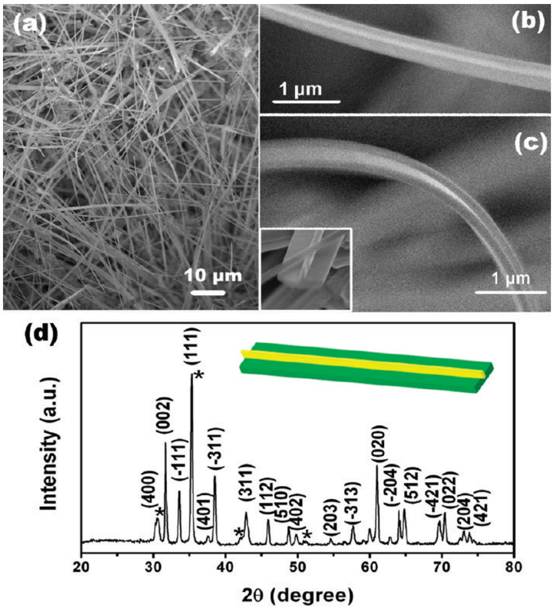

Figure 1. (a) Low-magnification SEM image of a product. (b, c) High-magnification SEM images of an individual heterostructure revealing the T-shaped cross-section (the inset). (d) XRD pattern of the product.

V/μm) and a high field-enhancement factor (over 4000). Due to their special geometry and enhanced conductivities the field-emission properties of the present nanomaterials not only surpass those of pure Ga_2O_3 and In_2O_3 components but also rival those of many other prospective 1D nanostructures. The novel structures are envisaged to become highly valuable in field-emitters and electrical and optoelectronic nanodevices.

RESULTS AND DISCUSSION

After the synthesis, wirelike products were found on the copper foil substrate. The product morphology was checked using scanning electron microscopy (SEM). Figure 1a shows a low-magnification SEM image of the material. It contains numerous whiskers with lengths ranging from several tens to hundreds of micrometers. High-magnification images (Figure 1b,c) reveal that a typical whisker, with a diameter of ~300 nm and a length of up to ~60 μm, displays a somewhat unusual appearance (see also the Supporting Information, Figure S1). Each heterostructure consists of a nanobelt and the nanowire located on its back forming a sort of a "dorsal fin"; thus, it shows the overall T-shaped cross-section (Figure 1c, inset). Further investigations by transmission electron microscopy (TEM) and X-ray energy dispersive spectroscopy (EDS) suggest that most of the whiskers (more than 80% of the product) are indeed such Ga_2O_3/In_2O_3 heterostructures, where the nanobelts and nanowires are made of Ga_2O_3 and In_2O_3, respectively (shown later). An X-ray diffraction (XRD) pattern of a product is shown in Figure 1d. Most of the strong peaks can be indexed to a monoclinic structure of Ga_2O_3 (JCPDS 76-573). Besides those peaks, some small peaks marked with star symbols are attributed to a cubic In_2O_3 phase (JCPDS 6-416).

The product morphology and microstructures were thoroughly studied using TEM, EDS, and selected area electron diffraction (SAED). Figure 2a is a typical TEM image of an individual heterostructure with a uniform width of 250 nm. The heterostructure appears to exhibit an inner "core" with a diameter of ~50 nm. In fact, the inner "core" of a dark contrast in TEM images actually represents the protuberant "dorsal fin" region along the axial direction. EDS spectra collected from the center and edge of the heterostructures (Figure 2b,c) show that the centers are composed of Ga, In, and O, whereas the edge only contains Ga and O. The SAED pattern of the heterostructure (Figure 2a, inset) can be indexed to the [110] zone axis of β-Ga_2O_3 and $[1\bar{2}1]$ zone axis of In_2O_3. Thus, the crystallographic relationship is that the [110] zone axis of a Ga_2O_3 belt is parallel to the $[1\bar{2}1]$ zone axis of an In_2O_3 wire. Figure 2d is a high-resolution TEM image taken from the edge of the Ga_2O_3 nanobelt. It clearly shows a single-crystalline characteristic. The *d* spacings of 0.267 and 0.282 nm correspond well to the (−111) and (002) plane separations in Ga_2O_3, respectively. The upper-right inset displays the corresponding 2D-Fourier transform (FFT) pattern. All reflections can be assigned to the [110] zone axis of a β-Ga_2O_3. An HRTEM image taken from the interface region of the Ga_2O_3 nanobelt/In_2O_3 nanowire is shown in

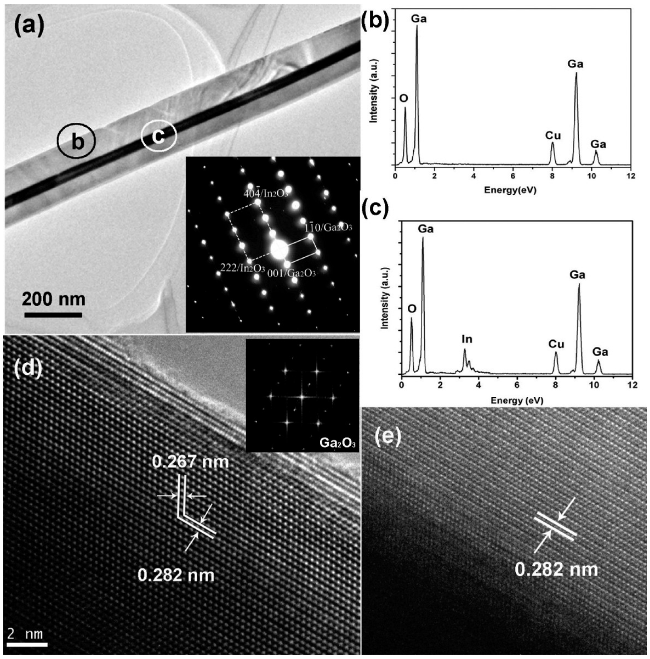

Figure 2. (a) Typical TEM image of a heterostructure; (inset) the corresponding SAED pattern, revealing the crystallographic relationship between a Ga_2O_3 nanobelt and the In_2O_3 nanowire. (b,c) EDS spectra taken from the labeled regions, showing that the center is composed of Ga, In, and O, whereas the edge only contains Ga and O. (d) HRTEM image recorded from the edge of the nanobelt implying its single-crystalline character; (inset) an FFT pattern corresponding to the HRTEM image in panel (d). (e) HRTEM image taken from the nanobelt/nanowire interface region.

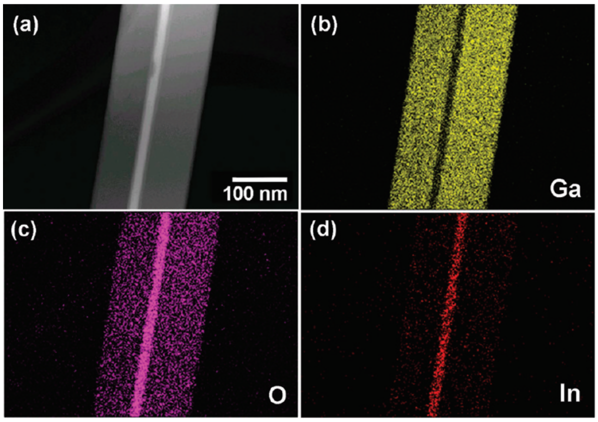

Figure 3. (a) HAADF STEM image of a heterostructure. (b−d) The spatially resolved Ga, In, and O elemental maps.

Figure 2e. The nontransparent dark region can be attributed to an impermeability of the 300 kV electron beam, indicating that a thickness of the protuberant heterostructure region is more than 100 nm.

A detailed chemical analysis was carried out using high-angle annular dark-field (HAADF) scanning transmission electron microscopy (STEM) and EDS elemental mappings. Figure 3a presents a HAADF STEM image of a heterostructure. The clear bright contrast regions naturally reflect the spatial distribution of In species (In has a larger atomic number than Ga). The elemental maps displayed in Figure 3b−d shed light on the distribution of the constituting elements, which are Ga, In, and O. The strong In L-edge signal originates from the In_2O_3 wire. The results clearly demonstrate a well-defined compositional profile of the Ga_2O_3/In_2O_3 heterostructure.

The formation of an In_2O_3-decorated Ga_2O_3 heterostructure proceeds via a one-step vapor−solid (VS) growth process. The whole growth process can be proposed as shown in Figure 4. At a high temperature, the reaction between Ga_2O_3 and activated carbon takes place as follows: Ga_2O_3 (solid) + 2C (solid) $\rightarrow$ Ga_2O (vapor) + 2CO (vapor) and $2Ga_2O$ (vapor) + 4CO (vapor) $\rightarrow$ 4Ga (vapor) + C (solid) + $3CO_2$ (vapor).[24] The newly generated Ga or Ga_2O vapors mix with the In vapor (coming from the starting material) and reach the substrate surface. Through the reaction with residual oxygen in the reaction system, Ga_2O_3 and In_2O_3 clusters are simultaneously formed and act as the nuclei for Ga_2O_3 and In_2O_3 nanowires. Then the heteroepitaxial growth of 1D Ga_2O_3/In_2O_3 nanowires occurs due to the lattice match between the two crystals at specific orientations. As aforementioned, the [111] zone axis of the Ga_2O_3 nanowire is parallel to the $[1\bar{2}1]$ zone axis of the In_2O_3 nanowire. At the same time, the excessive Ga_2O_3 clusters may deposit on the side surface of the formed Ga_2O_3 nuclei to ensure low energy growth.[25] With an increase in reaction time, the present In_2O_3-decorated Ga_2O_3 heterostructures are formed. Typical SEM images of products obtained after different reaction times (Figure S2, Supporting Information) clearly indicate that the heteroepitaxial growth of 1D heterostructures takes place at very early stages and then finally yields a product with a high aspect ratio.

Field-effect transistors (FETs) based on individual In_2O_3-decorated Ga_2O_3 heterostructures were fabricated, and their electrical properties were studied. The parallel Ti/Au electrodes, ~3 μm apart, were fabricated on a single heterostructure, as shown in Figure 5a. Figure 5b presents the gate-dependent drain-source current (I_{ds}) versus voltage (V_{ds}) curves recorded on a representative single FET device. The FET device exhibits notable gate dependence and is conductive, reaching a current of 3.4 μA with a V_{ds} of 10 V and a gate voltage (V_g) of 40 V. The nonlinear curves indicate that Schottky barriers form between the Ti/Au electrodes and the heterostructure. With a positively increasing V_g (−40 V→ 40 V), the conductance of the heterostructure increases, revealing an n-type conductivity. It has been reported that the pure Ga_2O_3 nanowires are normally n-type semiconductors due to oxygen vacancies.[14] In this work, the In_2O_3-decorated Ga_2O_3 heterostructures exhibit similar n-type semiconducting behavior. In addition, we also studied the electrical properties of the fabricated devices at different temperatures, in vacuum. Figure 5c displays $I_{ds}-V_{ds}$ curves measured from 300 to 10 K with $V_g = 0$ V. It can be seen that the conductance of a device decreases as the temperature decreases.

We further estimate the carrier concentration and mobility in the heterostructures. The conventional method to obtain such parameters is to analyze its field-effect behavior using a FET setup. However, herein the Schottky barriers play an important role in the electron transport and the FET model may result in an underestimate of the mobility.[26] In fact, the present device, as a metal−semiconductor−metal (MSM) structure, can be modeled by two Schottky barriers connected back to back, in series, with a resistor in between. Considering the tunneling current to become

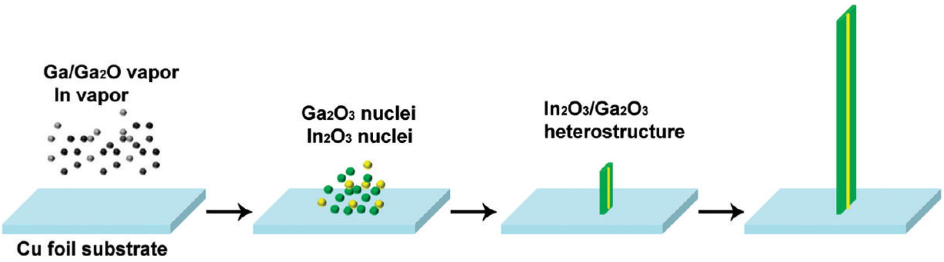

Figure 4. Schematic diagram of the growth of In_2O_3-decorated Ga_2O_3 heterostructures.

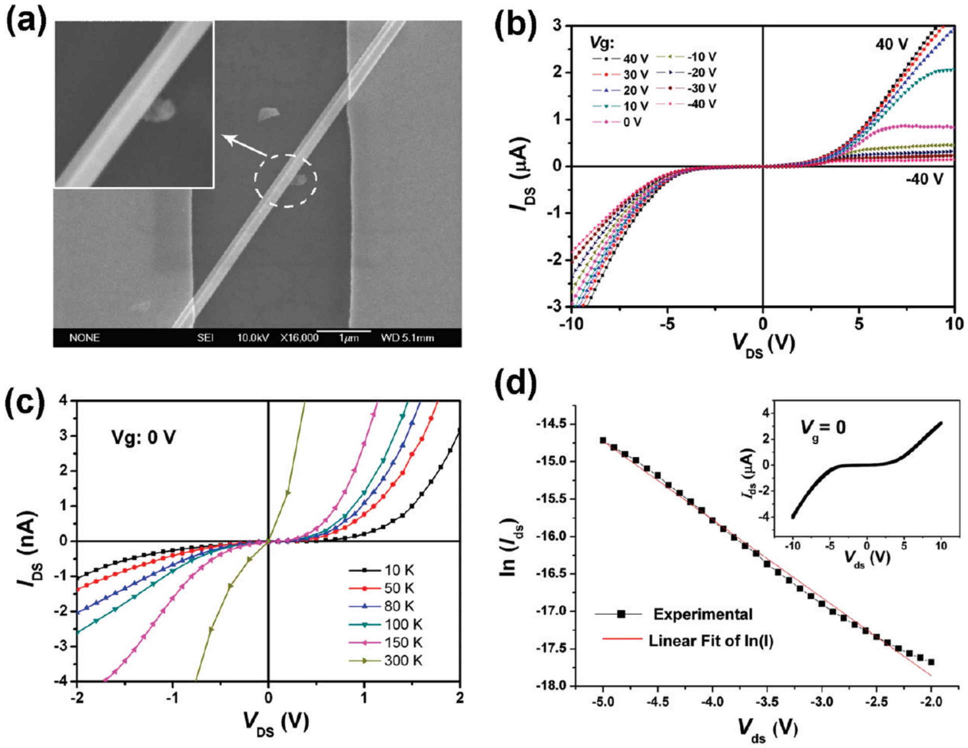

Figure 5. (a) SEM image of an In_2O_3-decorated Ga_2O_3 heterostructure-based FET; (inset) high-magnification SEM image showing the morphology of the heterostructure. (b) $I_{ds}-V_{ds}$ plots at different V_g. (c) $I_{ds}-V_{ds}$ curves measured from 300 to 10 K with $V_g = 0$ V. (d) Experimental and fitted ln*I* vs *V* plots at an intermediate bias using the $I_{ds}-V_{ds}$ curve at $V_g = 0$ (inset).

dominant under a reverse bias in a low-dimensional system, thermionic field emission theory is proposed for analyzing the present semiconductor parameters from the two-terminal $I-V$ curves.[26,27] In detail, the reverse-biased Schottky barrier dominates the total current I in the intermediate bias regime of the $I_{ds}-V_{ds}$ curve ($V_g = 0$)

$$\ln I = \ln(SJ) = \ln S + V\left(\frac{q}{kT} - \frac{1}{E_0}\right) + \ln J_S$$

where J is the current density through the Schottky barrier, S is the contact area, J_S is a slowly varying function of an applied bias, and $E_0 = E_{00}\coth(qE_{00}/kT)$ with $E_{00} = \hbar/2[n/(m_n{}^*\varepsilon_S\varepsilon_0)]^{1/2}$, n is electron concentration, $m_n{}^*$ and ε_S are the effective mass of an electron and relative permittivity of the material, respectively, and ε_0 is the permittivity of free space.

The logarithmic plot of a current I as a function of a bias V gives approximately a straight line with a slope $q/(kT) - 1/E_0$, as shown in Figure 5d. Then n can be obtained *via* E_0, and the electron mobility can be calculated using $\mu = 1/(nq\rho)$, with ρ being the resistivity of the heterostructure, which can be estimated to be 0.5 $\Omega \cdot$cm. Applying this procedure to the $I-V$ curves and assuming the relevant physical constants, such as $m_n{}^*$ and ε_S (for Ga_2O_3, $m_n{}^* \approx 0.342\ m_e$, $\varepsilon_S \approx 10$; for In_2O_3, $m_n{}^* \approx 0.3\ m_e$, $\varepsilon_S \approx 8.9$, m_e being the free electron mass[28−30]), the electron concentration of the heterostructure is estimated to be $(4.3-5.5) \times 10^{17}$ cm^{-3}, and the electron mobility is calculated to be 23−29 cm^2 V^{-1} s^{1-}. We also fabricated standard Ga_2O_3 nanobelts under the same reaction conditions but without the use of In reactant and studied their electrical properties (Supporting Information, Figure S3). The resistivity, electron concentration, and mobility in the synthesized Ga_2O_3 nanobelts was estimated to be 10.87 $\Omega \cdot$cm, 1.77×10^{17} cm^{-3}, and 3.2 cm^2 V^{-1} s^{1-}, respectively. It clearly indicates that the In_2O_3/Ga_2O_3 heterostructures possess significantly lower resistivity (0.5 $\Omega \cdot$cm) (higher conductivity) compared with pure Ga_2O_3 nanobelts (10.87 $\Omega \cdot$cm) as well as Ga_2O_3 nanowires (300−500 $\Omega \cdot$cm) in ref 14. In addition, the electron concentration in an In_2O_3/Ga_2O_3 heterostructure is much higher than in a pure Ga_2O_3 nanobelt. The present carrier mobility in the In_2O_3/Ga_2O_3 heterostructures (23−29 cm^2 V^{-1} s^{1-}) is about 1 order of magnitude higher than in a standard Ga_2O_3 nanobelt (3.2 cm^2 V^{-1} s^{1-}) and is also larger than in normal Ga_2O_3 nanowires (6.54 cm^2 V^{-1} s^{1-}) in ref 31. Therefore, on the basis of the above comparison, it is believed that the electrical behavior of the present heterostructures is greatly modulated by the In_2O_3 nanowire decoration. In particular, the In_2O_3 nanowires likely participate in the electron transport together with the Ga_2O_3 nanobelts. In addition, the trace amounts of In dopants into Ga_2O_3 nanobelts as well as the interface effect within the heterostructure may also contribute to the present electrical conductivity. Although the detailed electrical transport mechanism is

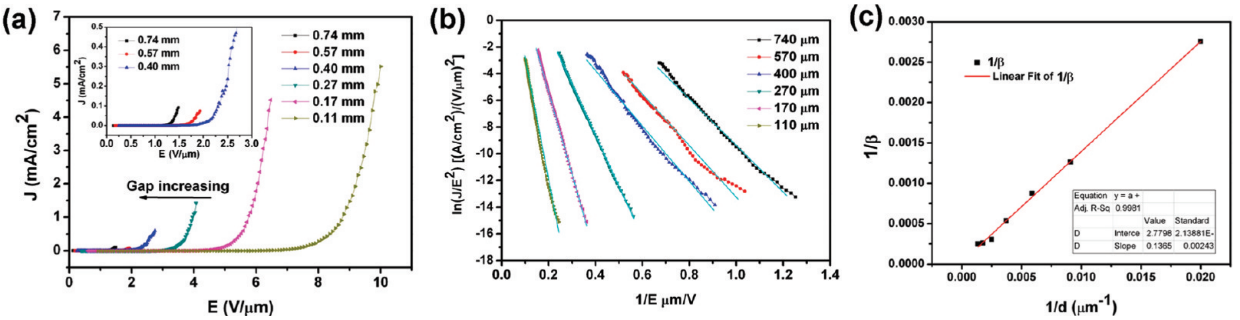

Figure 6. Field-emission properties of the heterostructures. (a) Field-emission current density versus an applied field ($J-E$) curves and (b) corresponding Fowler−Nordheim (FN) plots with different vacuum gaps. (c) Relationship between the field-enhancement factor, β, and a vacuum gap, d. The straight line is the linear fit of the experimental data based on the TRFE model.

still needs further clarification, what we can conclude at present is that, in contrast with standard Ga_2O_3 nanostructures, the present Ga_2O_3-based heterostructures demonstrate an enhancement of electron mobility and conductivity. It has been reported that nanostructures with lower resistivity have a better field-emission performance, which is due to the better supply of electrons to the emitting surface.[32] Therefore, the electrical study results imply that the heterostructure may be a valuable field emitter.

In order to study the performance of the In_2O_3-decorated Ga_2O_3 heterostructures as a field emitter, field-emission properties were measured in a high vacuum of $\sim 4.0 \times 10^{-6}$ Pa. Figure 6a shows the emission current density as a function of the electrical field ($J-E$ plot) measured at different spacings (d) between the anode and a sample. When the gap is increased from 0.11 to 0.74 mm, the turn-on field (E_{to}), which is defined as the field required to produce a current density of 10 μA/cm^2, decreases monotonously from 6.45 to 1.31 V/μm (Table 1). The current density at 6.4 V/μm is as high as 4.5 mA/cm^2 at $d = 0.17$ mm, and no current saturation is observed. It worth noting that the much lower turn-on field and higher current density of field-emission have been obtained for the present heterostructures, compared with either pure Ga_2O_3 nanostructures[14,21,23] or In_2O_3 nanostructures,[33,34] as summarized in Table 2. The data suggest that the newly prepared material is a highly valuable field-emitter that rivals previously reported ZnO, ZnS, SiC, Si, and AlN nanowires/nanobelts.[35]

The field-emission current−voltage characteristics were further analyzed using the Fowler−Nordheim (FN) theory

$$J = (A\beta^2E^2/\phi)\exp(-B\phi^{3/2}/\beta E)$$

or

$$\ln(J/E^2) = \ln(A\beta^2/\phi) - B\phi^{3/2}/\beta E$$

where $A = 1.54 \times 10^{-6}$ A eV V^{-2}, $B = 6.83 \times 10^3$ eV$^{-3/2}$ V μm^{-1}, β is the field-enhancement factor, and ϕ is the work function of an emitting material. Figure 6b shows the FN plots with different vacuum gaps. The plots are approximately linear, indicating that the FN theory well fits the field-emission behavior of the sample. We can calculate β from the slope of the FN plots in Figure 6b. Considering that the work function of Ga_2O_3 is 4.8 eV, β increases from 793 to 4002 under an increasing vacuum gap from 0.11 to 0.74 mm (Table 1). The β value is significantly larger than for other reported Ga_2O_3 or In_2O_3 nanostructures, as also illustrated in Table 2.

β is an important parameter in describing field emission. Generally, the β values are related to the emitter geometry, crystal structure, vacuum gaps, and spatial distribution of emitting centers. Structures with a higher aspect ratio would exhibit stronger field emissions from a given nanostructured material.[35,36] The relationship between β and d is crucial for fabrication field-emission devices. Figure 6c is a relationship of 1/β and 1/d. It shows that β obviously depends on d with a relationship of $1/\beta \propto 1/d$. On the basis of the two-region field-emission model, we found that the experimental data are almost fitted to a straight line and can be approximated by $1/\beta = h/d + 1/\beta_0$, where h is a

TABLE 1. Turn-on Field (E_{to}) and Field-Enhancement Factor β Obtained at Different Vacuum Gaps (d)

d (mm)	0.11	0.17	0.27	0.40	0.57	0.74
E_{to} (V/μm)	6.45	4.23	2.89	1.975	1.7	1.31
β	793	1142	1875	3287	3827	4002

TABLE 2. Comparative Key Field-Emission Performance Parameters of the Present Heterostructures and the Conventional Ga_2O_3 and In_2O_3 Nanostructures Reported in the Literature[a]

material	turn-on field (V/μm)	β	ref
quasi-aligned Ga_2O_3 nanowires	6.2	880	14
Ga_2O_3−C nanocables	7.73		21
cactus-like Ga_2O_3 nanostructures	12.6	38.2	23
In_2O_3 nanowires	2.47 at 0.1 μA/cm^2	1810	33
In_2O_3 nanowires	7 and 10.7 at 1 μA/cm^2		34
In_2O_3/Ga_2O_3 heterostructures	1.31−6.45	793−4002	this work

[a] Here, the turn-on field is defined as the field required to produce a current density of 10 μA/cm^2. If the other values are used, then this is mentioned separately.

width of the field-emission region near the whisker surface and β_0 is the absolute amplification factor, which is intrinsically determined by the emitting surface and independent of h, and d is an applied voltage. By fitting the slope and intercept value, the h and β_0 can be determined as ~136 nm and ~4×10^4, respectively. The value of β_0 is remarkably larger than that of a CNT on an Fe tip ($\beta_0 = 2.5 \times 10^4$) or a CNT film growing on a Si wafer ($\beta_0 = 7900$),[37] ZnO nanorods grown on a Si substrate ($\beta_0 = 3738$),[38] and aligned CdS nanocone arrays ($\beta_0 = 4933$),[36] indicating excellent field enhancement in the present In_2O_3-decorated Ga_2O_3 structures.

The high field-enhancement and low turn-on field values indicate that the present In_2O_3-decorated Ga_2O_3 heterostructures, despite their submicrometer dimensions, possess excellent field-emission characteristics. As we discussed above, the improved electrical properties (increased conductivity and mobility) are important for the observed field emission behavior. We can conclude that a high aspect ratio, good crystallinity, special geometry, and enhanced conductivity are responsible for these field-emission characteristics. It is believed that the growth of the analogous heterostructures with reduced dimensions will be an effective route to further enhance their field-emission performance and obtain more efficient emitters.

CONCLUSIONS

Novel 1D In_2O_3-decorated Ga_2O_3 heterostructure whiskers were synthesized via a simple catalyst-free vapor-solid method. The heterostructure consists of a primary Ga_2O_3 nanobelt and the In_2O_3 nanowire (in a shape of a "dorsal fin") and as a whole displays the T-shaped cross-section. Field-effect transistors were fabricated based on individual In_2O_3/Ga_2O_3 heterostructures. These showed n-type characteristics. The heterostructures possess lower resistivity and higher electron mobility compared with pure Ga_2O_3 nanostructures. Field-emission measurements showed the remarkably low turn-on field of ca. 1.31 V/μm at a current density of 10 μA/cm^2 and a vacuum gap of 0.74 mm. The field-enhancement factor β was calculated to be over 4000. The excellent field-emission characteristics are attributed to a high aspect ratio, good crystallinity, special geometry, and high conductivity of the present heterostructures. This new material may have a high promise for novel field-emitting, electronic and optoelectronic nanodevices.

METHODS

The synthesis of In_2O_3/Ga_2O_3 heterostructures was carried out in a conventional horizontal furnace. A mixture of Ga_2O_3 (500 mg), In (100 mg), and activated carbon (50 mg) was put in a quartz boat. A copper foil (10 mm × 20 mm) was first cleaned using alcohol in an ultrasonic cleaner and then capped on the quartz boat horizontally. After the boat was transferred into a quartz tube mounted in the furnace, the system was purged with 200 sccm Ar gas for 1 h. Then the furnace was heated to 1000 °C in 30 min and kept at this temperature for 1 h with the Ar flow kept constant. After the system was cooled to room temperature, a brown product was found deposited onto the Cu substrate.

An as-prepared product was characterized by a scanning electron microscope (SEM, JEOL, JSM-6700F), a powder X-ray diffractometer (XRD, RIGAKU, Ultima III, 40 kV/40 mA with Cu Kα radiation), a 300 kV high-resolution field-emission transmission electron microscope (TEM, JEOL, JEM-3000F) equipped with an energy-dispersive X-ray analyzer (EDX), and a high-angle annular dark-field scanning transmission electron microscopy detector (HAADF-STEM) (JEOL JEM-3100FEF).

For the fabrication of FET, In_2O_3-decorated Ga_2O_3 heterostructures were first dispersed in alcohol and then deposited onto a thermally oxidized Si substrate covered with a 600 nm SiO_2 layer at a desired density. The Ti/Au (10 nm/100 nm) interdigitated electrodes were patterned on top of the heterostructures using optical lithography with the assistance of a predesigned mask and electron beam deposition.

The field-emission properties were studied at room temperature in a high vacuum chamber (3×10^{-6} Pa) using a 1 mm^2 cross-sectional area Al anode. A dc voltage sweeping from 100 to 1100 V was applied to the samples.

Acknowledgment. This work was supported by the International Center for Materials Nanoarchitectonics (MANA) of the National Institute for Materials Science (NIMS), Japan, and the Nanotechnology Network Project of the Ministry of Education, Culture, Sports, Science and Technology (MEXT), Japan. The authors are indebted to Mr. S. Hara, M. H. Sugaya, and Mr. K. Ohno for their technical assistances and kind help.

Supporting Information Available: Low- and high-magnification SEM images of In_2O_3/Ga_2O_3 heterostructures, SEM images of products obtained after different reaction times, and the electrical property analysis of pure Ga_2O_3 nanobelts synthesized under similar reaction conditions. This material is available free of charge via the Internet at http://pubs.acs.org.

REFERENCES AND NOTES

1. Gudiksen, M. S.; Lauhon, L. J.; Wang, J.; Smith, D. C.; Lieber, C. M. Growth of Nanowire Supperlattice Structures for Nanoscale Photonics and Electronics. *Nature* **2002**, *415*, 617–620.
2. Robinson, R. D.; Sadtler, B.; Demchenko, D. O.; Erdonmez, C. K.; Wang, L. W.; Alivisatos, A. P. Spontaneous Superlattice Formation in Nanorods Through Partial Cation Exchange. *Science* **2007**, *317*, 355–358.
3. Algra, R. E.; Verheijen, M. A.; Borgström, Feiner, L. F.; Immink, G.; Van Enckevort, W. J. P.; Vlieg, E.; Bakkers, E. P. A. M. Twinning Superlattices in Indium Phosphide Nanowires. *Nature* **2008**, *456*, 369–372.
4. Lauhon, L. J.; Gudiksen, M. S.; Wang, D.; Lieber, C. M. Epitaxial Core-Shell and Core-Multishell Nanowire Heterostructures. *Nature* **2002**, *420*, 57–61.
5. Yan, J.; Fang, X.; Zhang, L.; Bando, Y.; Gautam, U. K.; Dierre, B.; Sekiguchi, T.; Golberg, D. Structure and Cathodoluminescence of Individual ZnS/ZnO Biaxial Nanobelt Heterostructures. *Nano Lett.* **2008**, *8*, 2794–2799.
6. Yin, L. W.; Li, M. S.; Bando, Y.; Golberg, D.; Yuan, X.; Sekiguchi, T. Tailoring the Optical Properties of Epitaxially Grown Biaxial ZnO/Ge, and Coaxial ZnO/Ge/ZnO and Ge/ZnO/Ge Heterostructures. *Adv. Funct. Mater.* **2007**, *17*, 270–276.
7. Jiang, X.; Xiong, Q.; Nam, S.; Qian, F.; Li, Y.; Lieber, C. M. InAs/InP Radial Nanowire Heterostructures as High Electron Mobility Devices. *Nano Lett.* **2007**, *7*, 3214–3218.
8. Hu, J.; Chen, Z.; Sun, Y.; Jiang, H.; Wang, N.; Zou, R. ZnO-Si Side-to-Side Biaxial Nanowire Heterostructures with Improved Luminescence. *J. Mater. Chem.* **2009**, *19*, 7011–7015.

9. Yang, R.; Chueh, Y. L.; Morber, J. R.; Snyder, R.; Chou, L. J.; Wang, Z. L. Single-Crystalline Branched Zinc Phosphide Nanostructures: Synthesis, Properties and Optoelectronic Devices. *Nano Lett.* **2007**, *7*, 269–275.
10. Wang, D.; Qian, F.; Yang, C.; Zhong, Z.; Lieber, C. M. Rational Growth of Branched and Hyperbranched Nanowire Structures. *Nano Lett.* **2004**, *4*, 871–874.
11. Jung, Y.; Ko, D.; Agarwal, R. Synthesis and Structural Characterization of Single-Crystalline Branched Nanowire Heterostructures. *Nano Lett.* **2007**, *7*, 264–268.
12. Gautam, U. K.; Fang, X.; Bando, Y.; Zhan, J.; Golberg, D. Synthesis, Structure, and Multiply Enhanced Field-Emission Properties of Branched ZnS Nanotube-In Nanowire Core-Shell Heterostructures. *ACS Nano* **2008**, *2*, 1015–1021.
13. Fang, X.; Bando, Y.; Gautam, U. K.; Zhai, T.; Gradečak, S.; Golberg, D. Heterostructures and Superlattices in One-Dimensional Nanoscale Semiconductors. *J. Mater. Chem.* **2009**, *19*, 5683–5689.
14. Huang, Y.; Wang, Z.; Wang, Q.; Gu, C.; Tang, C.; Bando, Y.; Golberg, D. Quasi-Aligned Ga_2O_3 Nanowires Grown on Brass Wire Meshes and Their Electrical and Field-Emission Properties. *J. Phys. Chem. C* **2009**, *113*, 1980–1983.
15. Binet, L.; Gourier, D. Origin of the Blue Luminescence of β-Ga_2O_3. *J. Phys. Chem. Solids* **1998**, *59*, 1241–1249.
16. Li, Z.; De Groot, C.; Moodera, J. H. Gallium Oxide as an Insulating Barrier for Spin-Dependent Tunneling Junctions. *Appl. Phys. Lett.* **2000**, *77*, 3630–3632.
17. Ogita, M.; Higo, K.; Nakanishi, Y.; Hatanaka, Y. Ga_2O_3 Thin Film for Oxygen Sensor at High Temperature. *Appl. Surf. Sci.* **2001**, *175*, 721–725.
18. Arnold, S. P.; Prokes, S. M.; Perkins, F. K.; Zaghloul, M. E. Design and Performance of a Simple, Room-Temperature Ga_2O_3 Nanowire Gas Sensor. *Appl. Phys. Lett.* **2009**, *95*, 103102.
19. Huang, Y.; Yue, S.; Wang, Z.; Wang, Q.; Shi, C.; Xu, Z.; Bai, X. D.; Tang, C.; Gu, C. Preparation and Electrical Properties of Ultrafine Ga_2O_3 Nanowires. *J. Phys. Chem. B* **2006**, *110*, 796–800.
20. Dai, Z. R.; Pan, Z. W.; Wang, Z. L. Gallium Oxide Nanoribbons and Nanosheets. *J. Phys. Chem. B* **2002**, *106*, 902–904.
21. Zhan, J.; Bando, Y.; Hu, J.; Li, Y.; Golberg, D. Synthesis and Field-Emission Properties of Ga_2O_3-C Nanocables. *Chem. Mater.* **2004**, *16*, 5158–5161.
22. Wang, Y.; Hou, L.; Qin, X.; Ma, S.; Zhang, B.; Gou, H.; Gao, F. Fabrication of Single-Crystalline β-Ga_2O_3 Nanowires and Zigzag-Shaped Nanostructures. *J. Phys. Chem. C* **2007**, *111*, 17506–17511.
23. Cao, C.; Chen, Z.; An, X.; Zhu, H. Growth and Field Emission Properties of Cactus-Like Gallium Oxide Nanostructures. *J. Phys. Chem. C* **2008**, *112*, 95–98.
24. Shen, G.; Chen, D.; Chen, P. C.; Zhou, C. Vapor-Solid Growth of One-Dimensional Layer-Structured Gallium Sulfide Nanostructures. *ACS Nano* **2009**, *3*, 1115–1120.
25. Hu, J.; Li, Q.; Zhan, J.; Jiao, Y.; Liu, Z.; Ringer, S. P.; Bando, Y.; Golberg, D. Unconventional Ribbon-Shaped β-Ga_2O_3 Tubes with Mobile Sn Nanowire Fillings. *ACS Nano* **2008**, *2*, 107–112.
26. Zhang, Z.; Yao, K.; Liu, Y.; Jin, C.; Liang, X.; Chen, Q.; Peng, L. M. Quantitative Analysis of Current-Voltage Characteristics of Semiconducting Nanowires: Decoupling of Contact Effects. *Adv. Funct. Mater.* **2007**, *17*, 2478–2489.
27. Zhang, Z. Y.; Jin, C. H.; Liang, X. L.; Chen, Q.; Peng, L. M. Current-Voltage Characteristics and Parameter Retrieval of Semiconducting Nanowires. *Appl. Phys. Lett.* **2006**, *88*, 073102.
28. He, H.; Orlando, R.; Blanco, M. A.; Pandey, R. First-Principles Study of the Structural, Electronic, and Optical Properties of Ga_2O_3 in its Monoclinic and Hexagonal Phases. *Phys. Rev. B* **2006**, *74*, 195123.
29. Oshima, T.; Okuno, T.; Arai, N.; Suzuki, N.; Hino, H.; Fujita, S. Flame Detection by a β-Ga_2O_3-Based Sensor. *Jpn. J. Appl. Phys.* **2009**, *48*, 011605.
30. Zeng, F.; Zhang, X.; Wang, J.; Wang, L.; Zhang, L. Large-Scale Growth of In_2O_3 Nanowires and Their Optical Properties. *Nanotechnology* **2004**, *15*, 596–600.
31. Li, Z.; Zhao, B.; Liu, P.; Zhang, Y. Synthesis of Gallium Oxide Nanowires and Their Electrical Properties. *Microelectron. Eng.* **2008**, *85*, 1618−1620; **2010**, *87*, 690.
32. She, J.; Xiao, Z.; Yang, Y.; Deng, S.; Chen, J.; Yang, G.; Xu, N. Correlation Between Resistance and Field Emission Performance of Individual ZnO One-Dimensional Nanostructures. *ACS Nano* **2008**, *2*, 2015–2022.
33. Kar, S.; Chaudhuri, S. Synthesis, Photoluminescence and Field Emission Properties of In_2O_3 Nanowires. *Chem. Phys. Lett.* **2006**, *422*, 424–428.
34. Li, S. Q.; Liang, Y. X.; Wang, T. H. Nonlinear Characteristics of the Fowler-Nordheim Plot for Field Emission From In_2O_3 Nanowires Grown on InAs Substrate. *Appl. Phys. Lett.* **2006**, *88*, 053107.
35. Fang, X.; Bando, Y.; Gautam, U. K.; Ye, C.; Golberg, D. Inorganic Semiconductor Nanostructures and Their Field-Emission Applications. *J. Mater. Chem.* **2008**, *18*, 509–522.
36. Zhai, T.; Fang, X.; Bando, Y.; Liao, Q.; Xu, X.; Zeng, H.; Ma, Y.; Yao, J.; Golberg, D. Morphology-Dependent Stimulated Emission and Field Emission of Ordered CdS Nanostructure Arrays. *ACS Nano* **2009**, *3*, 949–959.
37. Zhong, D. Y.; Zhang, G. Y.; Liu, S.; Sakurai, T.; Wang, E. G. Universal Field-Emission Model for Carbon Nanotubes on a Metal Tip. *Appl. Phys. Lett.* **2002**, *80*, 506–508.
38. Li, C.; Fang, G. J.; Liu, N. S.; Li, J.; Liao, L.; Su, F. H.; Li, G. H.; Wu, X. G.; Zhao, X. Z. Structural, Photoluminescence, and Field Emission Properties of Vertically Well-Aligned ZnO Nanorod Arrays. *J. Phys. Chem. C* **2007**, *111*, 12566–12571.